

Role of phonon scattering in graphene nanoribbon transistors: Nonequilibrium Green's function method with real space approach

Cite as: Appl. Phys. Lett. **98**, 203503 (2011); <https://doi.org/10.1063/1.3589365>

Submitted: 15 February 2011 . Accepted: 13 April 2011 . Published Online: 16 May 2011

Youngki Yoon, Dmitri E. Nikonov, and Sayeef Salahuddin



View Online



Export Citation

ARTICLES YOU MAY BE INTERESTED IN

[Phonon limited transport in graphene nanoribbon field effect transistors using full three dimensional quantum mechanical simulation](#)

Journal of Applied Physics **112**, 094505 (2012); <https://doi.org/10.1063/1.4764318>

[Single and multiband modeling of quantum electron transport through layered semiconductor devices](#)

Journal of Applied Physics **81**, 7845 (1997); <https://doi.org/10.1063/1.365394>

[Mode space approach for tight-binding transport simulations in graphene nanoribbon field-effect transistors including phonon scattering](#)

Journal of Applied Physics **113**, 144506 (2013); <https://doi.org/10.1063/1.4800900>

Lock-in Amplifiers up to 600 MHz

starting at

\$6,210



Zurich Instruments

Watch the Video



Role of phonon scattering in graphene nanoribbon transistors: Nonequilibrium Green's function method with real space approach

Youngki Yoon,¹ Dmitri E. Nikonov,² and Sayeef Salahuddin^{1,a)}

¹Department of Electrical Engineering and Computer Sciences, University of California, Berkeley, California 94720, USA

²Technology and Manufacturing Group, Intel Corp., SC1-05, Santa Clara, California 95052, USA

(Received 15 February 2011; accepted 13 April 2011; published online 16 May 2011)

We report self-consistent NEGF transport simulation results in graphene nanoribbon transistors with phonon scattering in real space. Unlike mode space approach, this technique can account for interband scattering in addition to intraband scattering. We show a seamless transition from ballistic to dissipative transport by varying channel length over a wide range. We find acoustic phonon (AP) scattering to be the dominant scattering mechanism within the relevant range of voltage bias. Optical phonon scattering is significant only when a large gate voltage is applied. In a longer channel device, the contribution of AP scattering to the dc becomes more significant. © 2011 American Institute of Physics. [doi:10.1063/1.3589365]

A quasi-one-dimensional strip of carbon, graphene nanoribbon (GNR), has been intensively explored for the potential applications of field-effect transistors (FETs), resulting in promising experimental demonstrations.¹⁻³ In order to understand the unique transport mechanism in GNR, self-consistent atomistic quantum simulations have been performed within ballistic approximation.⁴⁻⁶ In practice, however, long channel GNR-FETs show dissipative transport,⁷ which indicates that scattering mechanisms should be considered in realistic device simulations. Interestingly, electron-phonon scattering cannot be overlooked even for a relatively short channel GNR-FET, as will be shown in this work.

Dissipative transport simulations of GNR-FETs as well as carbon nanotube (CNT) FETs have been performed so far by means of mode space approach,⁸⁻¹⁰ which is computationally favorable. However, mode space approach, which is effective for intraband scattering [Fig. 1(a)], has a limitation in taking interband scattering [Fig. 1(b)] into account since each subband is treated independently of another. Note that even for a 2 nm wide GNR ($N_a=16$ armchair-edge GNR as used in this study), the energy difference between the first and the second lowest subband is only 160 meV. The coupling between the subbands caused by phonon scattering would become more significant and complicated as GNR width increases. Therefore, in this study, we use real space approach to treat all possible couplings between the subbands.

Device characteristics are calculated from the self-consistent solution of the three-dimensional Poisson equation and the nonequilibrium Green's function (NEGF) equations with tight-binding approximation in the p_z orbital basis set.¹¹ The model device structure has $N_a=16$ armchair-edge GNR ($E_g=0.7$ eV) for the channel material. N-doped source and drain are 30 nm long, respectively, with a doping density of 0.5 dopant per nm or equivalently $2.6 \times 10^{13}/\text{cm}^2$. Channel length is varied from 30 to 240 nm. Double-gate geometry is used with 2.5 nm thick HfO_2 ($\kappa=16$) dielectric material. Power supply voltage of $V_{DD}=0.3$ V and $T=300$ K are assumed.

In order to model phonon scattering, in- and out-scattering self-energies are introduced as follows:

$$\Sigma_S^{in/out}(E) = D_\omega \{N_\omega(E) + 1\} G^{n/p}(E \pm \hbar\omega) + D_\omega N_\omega(E) G^{n/p}(E \mp \hbar\omega), \quad (1)$$

where D_ω is electron-phonon coupling constant, N_ω is phonon occupation number in thermal equilibrium, and $G^{n(p)}$ is electron (hole) correlation function.¹¹ In this study, D_ω is calculated from electron-phonon interaction Hamiltonian¹²⁻¹⁴ ($D_{\omega,AP}=0.01$ eV² and $D_{\omega,OP}=0.07$ eV² with $\hbar\omega=196$ meV). In the presence of phonon scattering, scattering self-energy adds additional complexity in a full self-consistent simulation. Unlike a ballistic transport, two iterative loops are needed for the solution of the transport equation since Green's function and scattering self-energy affect each other: one for elastic scattering and the other for inelastic scattering. One iterative loop is required for the treatment of elastic scattering and the other is needed for inelastic scattering.

In general, phonon scattering has a negative impact on the dc of a transistor since a portion of scattered carriers travel back to the source and cannot reach the drain. First, we plotted basic device characteristics under ballistic and dissipative transport for GNR-FETs with a fixed channel length, $L_{ch}=30$ nm (Fig. 2). Figures 2(a) and 2(b) show that acoustic phonon (AP) scattering is a dominant scattering mechanism within the normal bias range if we define $V_{off}=0.2$ V and $V_{on}=0.5$ V with $V_{DD}=0.3$ V. From both plots, we observe that current is decreased by roughly 14% in the presence of AP scattering. Optical phonon (OP) scattering adds

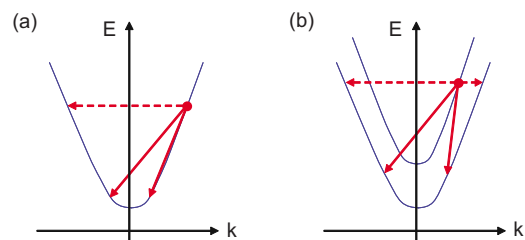


FIG. 1. (Color online) Schematic plot of (a) intraband and (b) interband scattering. Dashed and solid arrows illustrate elastic and inelastic scattering, respectively.

^{a)}Electronic mail: sayeef@eecs.berkeley.edu.

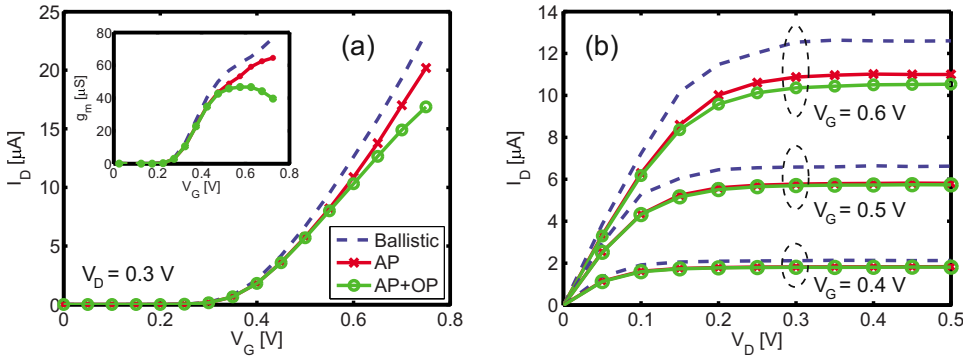


FIG. 2. (Color online) (a) I_D - V_G curve at $V_D=0.3$ V. Transconductance $g_m(=\partial I_D/\partial V_G)$ versus V_G plot is shown in the inset. (b) I_D - V_D plot at $V_G=0.4, 0.5$, and 0.6 V. Dashed lines, solid lines with crosses, and solid lines with circles are for ballistic transport, with AP scattering, and with both AP and OP scattering, respectively.

only a negligible difference in current compared to AP scattering up to $V_G=0.5$ V. It is significant only when a higher gate voltage is applied.¹⁰ At $V_G=0.75$ V, the contribution of OP to the current becomes comparable to that of AP, for the case of $L_{ch}=30$ nm. Transconductance, $g_m=\partial I_D/\partial V_G$ is, however, significantly influenced by OP scattering. The inset of Fig. 2(a) shows that OP scattering limits the transconductance and the maximum g_m can be reached at a lower gate voltage, as compared to the other two cases.

Bias-dependent phonon contribution can be understood by plotting current flow. Figures 3(a) and 3(b) show energy-resolved current spectrum along the device at $V_G=0.4$ V and 0.6 V, respectively. OP scattering is suppressed at $V_G=0.4$ V since the energy window for current flow in the channel is smaller than the phonon energy [Fig. 3(a)]. However, at $V_G=0.6$ V, a significant number of injected carriers have empty states available for scattering, and an OP can be emitted [solid arrow in Fig. 3(b)]. Note that the number of available states for OP scattering will increase as a larger gate voltage is applied, and therefore the impact of OP scattering will become more significant [Fig. 2(a)]. Figures 3(c) and 3(d) show energy-resolved current at the end of channel position ($x=60$ nm). Although both AP and OP scattering have been considered, at $V_G=0.4$ V, current is mostly affected by AP and the scattering is only an elastic event [Fig. 3(c)]. At $V_G=0.6$ V, however, it exhibits the signature of OP scattering where the spectrum is skewed down to the lower

energy levels [Fig. 3(d)]. The role of OP is clearly illustrated in Figs. 3(e) and 3(f), which are electron distribution plots under ballistic and dissipative transport, respectively. In the presence of OP scattering, electrons can populate certain energy levels that are forbidden in case of ballistic transport. Note that OP scattering in the drain has minor impact on the total current of the device [dashed arrows in Figs. 3(a) and 3(b)]. The reason is that, once OP is emitted in the drain region, it is very unlikely that electrons can travel back to the source due to the insufficient energy to overcome the potential barrier.

In Figs. 3(g) and 3(h), we have also shown energy-resolved current spectrum for a longer channel device ($L_{ch}=240$ nm) at $V_G=0.2$ V and 0.6 V, respectively, where we can see a more pronounced evidence of dissipative transport. The most prominent feature is a slanted potential profile at a high gate voltage [Fig. 3(h)], which is analogous to what one usually encounters in conventional metal-oxide-semiconductor (MOS) FETs. This indicates that our atomistic quantum transport simulation can accommodate seamless transition from ballistic to quasiballistic or dissipative transport as the dimension of the device increases. The slanted potential profile is due to the pile-up of electrons resulting from phonon scattering in the channel region. In most cases of OP scattering, phonon emission is a relevant mechanism to the transport, but at a low gate voltage, electrons that

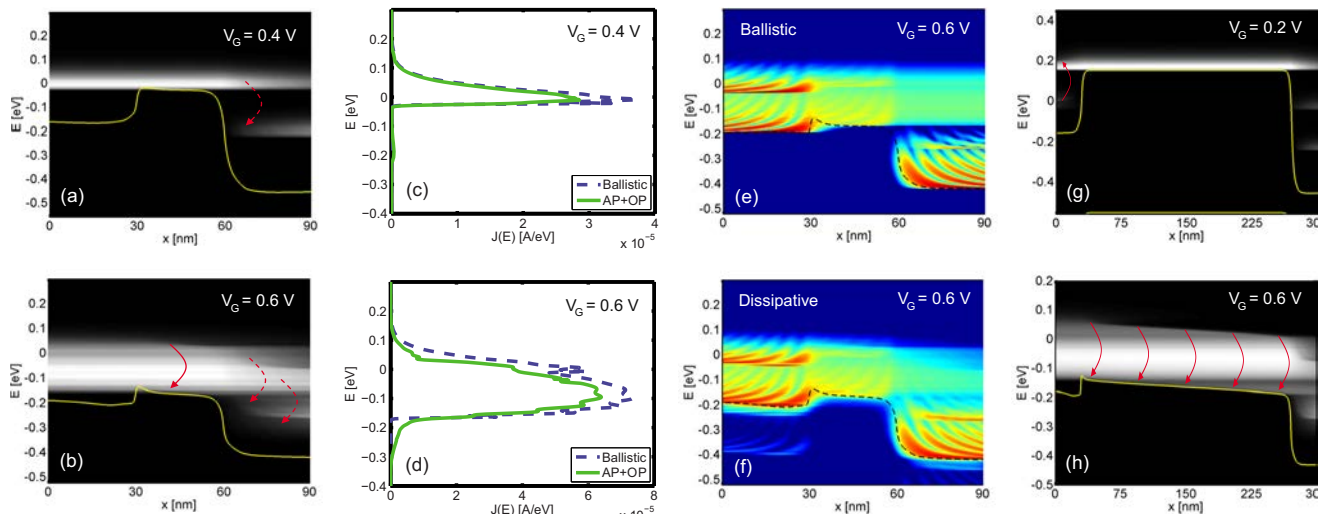


FIG. 3. (Color online) Energy-resolved current spectrum at (a) $V_G=0.4$ V and (b) 0.6 V in the presence of phonon scattering (both AP and OP are treated) for a $L_{ch}=30$ nm GNR-FET. Solid line shows conduction band profile E_c . Energy-resolved current at the channel-drain interface ($x=60$ nm) under ballistic (dashed line) and dissipative transport (solid line) at (c) $V_G=0.4$ V and (d) 0.6 V. Electron correlation function, G^2 plotted on a log scale, which shows electron distribution in energy and position, under (e) ballistic and (f) dissipative transport at $V_G=0.6$ V. Dashed line shows E_c . Energy-resolved current spectrum at (g) $V_G=0.2$ V and (h) 0.6 V under dissipative transport (with both AP and OP) for a $L_{ch}=240$ nm device. The arrows show OP scattering.

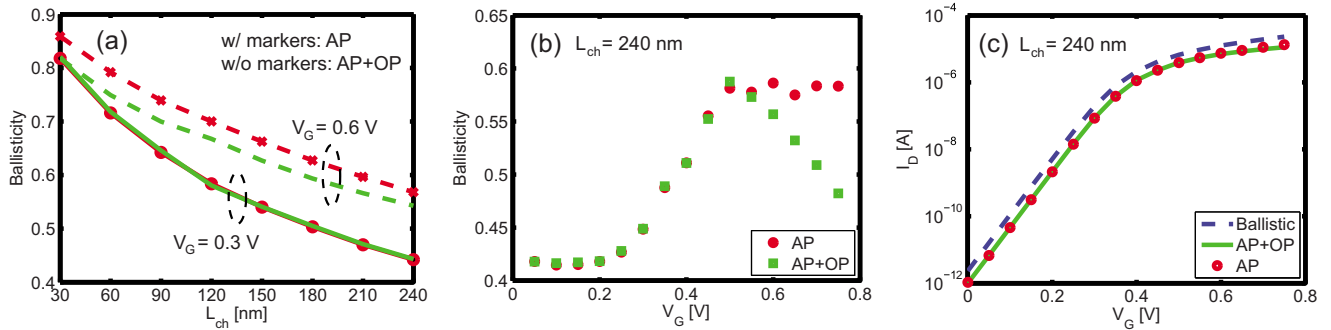


FIG. 4. (Color online) (a) Ballistic (I_{sca}/I_{bal}) as a function of channel length at two different gate voltages. (b) Ballistic as a function of gate voltage with AP scattering (circles) and both AP and OP scattering (squares) for a $L_{ch}=240$ nm device. (c) I_D-V_G plot for a $L_{ch}=240$ nm device under ballistic transport (dashed line), with AP scattering (circles), and with both AP and OP scattering (solid line).

absorb phonons can contribute to the total current of device, too [arrow in Fig. 3(g)].

Next, we have explored the impact of phonon scattering on different size of devices by plotting ballisticity, which is defined as the ratio of current in the presence of phonon scattering to ballistic current (I_{sca}/I_{bal}), in Fig. 4(a). Our simulation shows that ballisticity is decreased with channel length, which indicates that the effect of phonon scattering or the number of scattering events is enhanced as the channel length increases. Ballisticity also depends on the gate voltage for a given channel length. To better understand this voltage dependence, we have plotted ballisticity as a function of gate voltage for $L_{ch}=240$ nm [Fig. 4(b)]. The results are summarized as follows: first, the effect of OP is significant only at high gate voltages ($V_G > 0.55$ V), which is consistent with what we have observed in Fig. 2. However, in the long channel device (240 nm), the main contribution of phonon results from AP ($\sim 80\%$) even at $V_G=0.75$ V. The effect of OP scattering becomes minor ($\sim 20\%$) since most electrons that emit phonons in the long channel may not have sufficient energy to overcome the potential drop imposed by the slanted potential profile and finally exit to the drain [Fig. 3(h)]. Second, with AP scattering, ballisticity is gradually increased or equivalently the effect of phonon scattering is decreased when the gate bias achieves the threshold. This can be explained with (i) density of states (DOS) of one-dimensional system and (ii) scattering mechanism. At a low V_G , current flows mainly near the conduction band edge (E_c) where carriers experience large DOS and hence large scattering rate.¹⁵ In addition, since the second lowest subband is beyond the range of the relevant transport, carriers with positive wave vector must travel backward after an intraband elastic scattering event in this case. In contrast, however, at a high V_G , a considerable fraction of carriers flow well above the E_c and the scattering rate could be smaller at the relevant energy levels.¹⁵ At an increased gate voltage, the second lowest subband is involved in the transport and a portion of scattered carriers may travel forward even after a scattering event due to interband elastic scattering, which may further increase ballisticity. Third, the ballisticity is almost constant in the subthreshold region, which implies the $\log_{10}(I_D)-V_G$

curve can be shifted parallel by AP scattering. Figure 4(c) confirms this; threshold voltage is shifted by $\Delta V_t=23$ mV, which could be more significant if gate efficiency becomes worse.

To summarize, we have studied the effect of phonon scattering in GNR-FETs by using self-consistent atomistic quantum transport simulation based on NEGF formalism with real space approach. Our simulation results show seamless transition from ballistic to dissipative transport by varying the simulated device size. AP scattering has a major impact on the current degradation within the relevant range of voltage operation while OP scattering is significantly suppressed unless a high gate voltage is applied. At a high V_G , the effect of AP scattering on the dc is reduced thanks to lower DOS at the relevant energy levels and the contribution from the upper subband while OP scattering simply affects negatively the on current of the device.

This work was supported in part by FCRP center on FENA and NSF.

¹M. Han, B. Ozyilmaz, Y. Zhang, and P. Kim, *Phys. Rev. Lett.* **98**, 206805 (2007).

²Z. Chen, Y. Lin, M. Rooks, and P. Avouris, *Physica E (Amsterdam)* **40**, 228 (2007).

³X. Li, X. Wang, L. Zhang, S. Lee, and H. Dai, *Science* **319**, 1229 (2008).

⁴Y. Ouyang, Y. Yoon, and J. Guo, *IEEE Trans. Electron Devices* **54**, 2223 (2007).

⁵G. Fiori and G. Iannaccone, *IEEE Electron Device Lett.* **28**, 760 (2007).

⁶G. C. Liang, N. Neophytou, M. S. Lundstrom, and D. E. Nikonov, *J. Appl. Phys.* **102**, 054307 (2007).

⁷X. Wang, Y. Ouyang, X. Li, H. Wang, J. Guo, and H. Dai, *Phys. Rev. Lett.* **100**, 206803 (2008).

⁸Y. Ouyang, X. Wang, H. Dai, and J. Guo, *Appl. Phys. Lett.* **92**, 243124 (2008).

⁹J. Guo, *J. Appl. Phys.* **98**, 063519 (2005).

¹⁰S. O. Koswatta, S. Hasan, M. S. Lundstrom, M. P. Anantram, and D. E. Nikonov, *IEEE Trans. Electron Devices* **54**, 2339 (2007).

¹¹S. Datta, *Quantum Transport: Atom to Transistor* (Cambridge University Press, Cambridge, 2005).

¹²G. D. Mahan, *Phys. Rev. B* **68**, 125409 (2003).

¹³S. Hasan, Ph.D. dissertation, Purdue University, 2005.

¹⁴D. Nikonov, H. Pal, and G. Bourianoff, "Electron-phonon and spin scattering in NEGF: Made simple," 2009, <http://nanohub.org/resources/7772>.

¹⁵S. O. Koswatta, S. Hasan, M. S. Lundstrom, M. P. Anantram, and D. E. Nikonov, *Appl. Phys. Lett.* **89**, 023125 (2006).